

Permittivity and remanent polarization contributions to the electrocaloric effect in (Ba, Sr)TiO₃ under unipolar field

Yukiya Tanaka¹, Ryo Iguchi^{2*}, Takashi Teranishi^{1, 3*}, Shinya Kondo¹, Akira Kishimoto¹,

¹Graduate School of Natural Science and Technology, Okayama University,
3-1-1 Tsushima-naka, Kita, Okayama 700-8530, Japan

²National Institute for Materials Science, 1-2-1 Sengen, Tsukuba 305-0047, Japan

³Laboratory for Materials and Structures, Tokyo Institute of Technology,
4259 Nagatsuta, Midori, Yokohama 226-8503, Japan

^{a)}Authors to whom correspondence should be addressed: IGUCHI.Ryo@nims.go.jp, teranishi@cc.okayama-u.ac.jp

Abstract

The electrocaloric effect (ECE)-induced temperature change (ΔT) in (Ba, Sr)TiO₃-based ferroelectrics under unipolar electric fields was analyzed from the separate contributions of the dielectric constant (ϵ) and remanent polarization (P_r) based on the Maxwell relation. Consideration of the contributions of both ϵ and P_r is particularly important in a unipolar electric field operation, such as on/off field switching used in device applications. Direct ΔT measurements were also performed based on the lock-in thermography technique to verify the accuracy of the ΔT intensity estimated by the indirect method. The indirect and direct ΔT values were largely consistent. The ΔT intensity near the peak temperature of ΔT was dominated by the P_r contribution; a large $\partial P_r / \partial T$ was necessary to increase the overall ΔT magnitude. In contrast, a large $\partial \epsilon / \partial T$ was essential to expand the operating temperature range of ΔT at temperatures higher than the dielectric maximum temperature. Quantitative understanding of the contributions of both ϵ and P_r to ΔT in unipolar electric fields is expected to guide the search for materials with a superior ECE.

A cooling system based on the electrocaloric effect (ECE) is a promising candidate for next-generation environmentally friendly electronic modules to replace the current vapor compression cycle-based systems, which use fluorite-based gases.^{1,2} The ECE is a heat absorption/generation phenomenon that results from variation in polarization entropy under a changing external electric field.³⁻⁹ The ECE can induce a temperature change (ΔT) under adiabatic conditions. The current highest value is approximately 10 K,¹⁰ which has been observed in ferroelectric thin films near the ferroelectric–paraelectric phase-transition temperature (T_c). Additionally, the coefficient of performance has been reported to exceed 10 for prototypical devices.^{11,12}

The ECE is discussed on the basis of ΔT under the external electric field.¹³ It is maximized around the dielectric maximum temperature (T_m), which involves the ferroelectric–paraelectric phase transition.¹⁴⁻¹⁶ The dielectric polarization includes the permittivity response and the remanent polarization (P_r). Thus, both the dielectric constant (ϵ) and P_r contribute to the polarization entropy change. It has been discussed that the P_r contribution is significant for the unipolar operation, such as on/off field switching.¹⁷ However, only a few studies have been dedicated to the indirect ECE measurements under unipolar electric fields¹⁸⁻²⁰, and the contributions of ϵ and P_r to the ECE have not yet been quantified.

Herein, we quantify the contributions of ϵ and P_r to ΔT in ECE materials under unipolar electric fields via a modified indirect ECE measurement (Fig. 1). The ΔT values are calculated from the temperature dependence (T -dependence) of the ϵ and P_r values obtained from P – E measurements under unipolar and bipolar electric fields. The estimated ΔT values are also compared with the directly measured ΔT using a field-modulated lock-in thermography technique (LIT),²¹⁻²³ which is performed simultaneously with the unipolar P – E measurements.

In the indirect measurement, the adiabatic $\Delta T_{\text{indirect}}$ due to the ECE is described by the Maxwell

relation.^{24,25} Based on the decomposition of polarization P with $P(E) = P_r + \varepsilon_0(\varepsilon-1)E$, it can be described by Equation (1) as follows:¹⁹

$$\Delta T_{\text{indirect}} = -\frac{T}{\rho \cdot C_p} \times \int_0^{E_{\text{max}}} \frac{\partial(\varepsilon_0(\varepsilon-1)E + P_r)}{\partial T} dE, \quad (1)$$

where ρ is the density, C_p is the specific heat, E (E_{max}) is the (maximum) electric field, and ε_0 is the vacuum permittivity. The T -dependences of ε and P_r are measured by a Sawyer–Tower circuit,²⁶ and each contribution is estimated in Equation (1).

ε and P_r are estimated as follows. To determine ε , a sinusoidal waveform that varies from 0 to E_{max} at the frequency, f , is used as an AC electric field according to Equation (2), as follows:

$$E(t) = E_{\text{max}} \times \left[\sin\left(\frac{2\pi ft}{2}\right) + \frac{1}{2} \right]. \quad (2)$$

Here, the obtained P – E hysteresis is unipolar. The waveform corresponds to turning the electric field on and off (as in real devices),^{12,27} and thus our direct measurements were also performed under this electric field. ε is estimated according to the approximation of $P(E_{\text{max}}) - P(0) = \varepsilon_0(\varepsilon-1)E_{\text{max}}$. P_r cannot be estimated for a unipolar hysteresis since the Sawyer–Tower circuit only measures the change in polarization. Thus, to estimate P_r , bipolar hysteresis, where the electric field varies from $-E_{\text{max}}$ to E_{max} , was also measured.²⁸ Bipolar hysteresis enables estimation of the absolute P value at E_{max} (P_{max}). The P_r value is estimated as $P_r = P_{\text{max}} - \varepsilon_0(\varepsilon-1)E_{\text{max}}$ (see Fig.1).

In the experiment, $\text{Ba}_{0.8}\text{Sr}_{0.2}\text{TiO}_3$ (08BST) was used because its T_m is in the vicinity of room temperature, i.e., 340 K; it was synthesized via a conventional solid-state reaction.²⁹ X-ray diffraction (Mini Flex, Rigaku) confirmed that the material was single phase, had tetragonal symmetry, and was impurity-free. The density was $5.56 \times 10^3 \text{ kg/m}^3$ measured by Archimedes method and the relative density was 95.2%. Figure 2(a) shows the T -dependence of C_p measured using Differential Scanning Calorimetry (DSCvesta, Rigaku). Pellets of 08BST were cut into cuboid pieces of dimensions $2.0 \times 2.0 \times 1.0 \text{ mm}^3$ using a step cutter for direct and indirect ECE measurements. Then, the specimens were

polished using lapping films of grits ranging from #400 to #10,000. Au electrodes (100-nm-thick) were sputter-deposited on the $2.0 \times 2.0 \text{ mm}^2$ surfaces, and 50- μm -thick Au wires were attached to the electrodes using Ag paste. The 08BST specimen was connected to a Sawyer–Tower circuit equipped with a 0.1- μF reference capacitor and placed on a temperature-controlled stage equipped with a Peltier module. The surface between the Au electrodes ($2.0 \times 1.0 \text{ mm}^2$) was observed using an infrared camera. The static component of the captured thermal image is used to determine the sample temperature, and the dynamic component is used to directly measure ΔT through LIT. The values in the following are averaged over the entire sample surface. Since it was confirmed that the sample surface exhibited sufficiently high emissivity, no coating was applied.²³

The measurements were carried out while the temperature was increased from approximately 320 to 350 K. Prior to the measurements, depolarization was achieved by increasing the temperature above the Curie temperature and then decreasing it to 320 K in the absence of an electric field. Subsequently, at each temperature, the unipolar hysteresis was measured along with simultaneous LIT-based direct measurements, followed by the bipolar hysteresis measurement. The frequency was set to 20 Hz, and the voltage was fixed at $E_{\text{max}} = 500 \text{ V}$, except during the electric field dependence measurements. In the data analysis, smoothing splines were used to determine the T derivative of the ε and P_r values.

Figure 2(b) shows the T dependence of ε and ECE-induced ΔT calculated only from ε (ΔT_ε) at $E_{\text{max}} = 500 \text{ V/mm}$. The T dependence of ε reached a maximum in the measurement temperature range, and T_m of 335.4 K was obtained by fitting the ε values around the peak with a quadratic function. In contrast, since ΔT_ε is proportional to $\partial\varepsilon/\partial T$, ΔT_ε shows negative and positive peaks, respectively, below and above T_m .

Figure 2(c) shows the P_r at $E_{\text{max}} = 500 \text{ V/mm}$ and ECE-induced ΔT calculated only from P_r (ΔT_{P_r}). The P_r value decreased with increasing T . The graph shows a peak maximum at about T_m . The actual peak temperature of ΔT_{P_r} was 333.5 K, which is lower than T_m .

Next, the T dependence of $\Delta T_{\text{indirect}}$ was calculated by adding ΔT_{P_r} and ΔT_{ε} [Figure 2(d)]. The $\Delta T_{\text{indirect}}$ displayed a positive peak with a maximum at 334.2 K. Notably, the peak temperature for $\Delta T_{\text{indirect}}$ differed from those for ΔT_{P_r} and ΔT_{ε} . Therefore, the contributions from both ε and P_r are indispensable when discussing the overall ECE. Below T_m , ΔT_{P_r} and ΔT_{ε} had opposite signs and thus weakened each other, whereas above T_m , the contributions were additive. The maximum $\Delta T_{\text{indirect}}$ value was primarily determined by the maximum ΔT_{P_r} value, since ΔT_{ε} was about zero near T_m .

The contributions of ε and P_r to $\Delta T_{\text{indirect}}$ are explained by the vanishing of P_r at elevated temperatures and the enhancement of ε near the Curie temperature. The P_r value kept decreasing with increasing temperature, and after the ferroelectric–paraelectric phase transition, the values became almost zero. In contrast, ε reached its maximum value at the T_m where the P_r was almost zero. This behavior is attributed to an electric field-induced phase transition in the BST at the T_m or higher temperature. Namely, dipole clusters originating from Ti displacement along the $\langle 111 \rangle$ orientation³⁰ are transformed into the macrodomain under the application of the high-intensity E field. The increment in the dipole contribution increased the ΔT_{ε} at higher temperatures, i.e., above the T_m .

We also performed LIT-based thermographic measurements to confirm the accuracy of the magnitude of the $\Delta T_{\text{indirect}}$ values. The LIT measurements were performed simultaneously with the unipolar P - E measurements at the lock-in frequency of 20 Hz. The lock-in frequency was confirmed to be sufficiently high to separate the contributions from leakage-induced Joule heating and thermal loss effect based on the frequency-dependence measurements conducted prior to the T -dependence measurements.²³ The ΔT obtained by direct measurement was defined as ΔT_{direct} ; Figure 2(d) indicates that the magnitudes of ΔT_{direct} and $\Delta T_{\text{indirect}}$ were comparable and in better agreement compared to previous study.¹⁹

The effect of E_{max} variation in the range of 100–1,000 V/mm on ECE characteristics was also investigated. A change in E_{max} changes both the amplitude and DC bias of the applied electric field

waveform. It has been established that the dielectric properties of ferroelectrics are significantly affected by DC bias, particularly due to the changes in dipole contributions associated with the domain structure.^{31,32} Thus, substantial changes in the ECE were expected when E_{\max} was changed.

Figure 3(a) shows ε for E_{\max} , ranging from 100 to 1,000 V/mm. With increasing E_{\max} , the ε value decreased, the peak intensity diminished, and the estimated T_m shifted to higher temperature. These behaviors are consistent with previous research.^{31,32} In normal ferroelectrics possessing a typical domain configuration, increasing the DC bias field intensity decreases ε as the domain wall motions.^{31,33,34} Although ε was lower at the elevated E_{\max} values, ΔT_ε still increased with increasing E_{\max} [Figure 3(b)]. This is because ΔT_ε is proportional to E^2 , as described in Equation (2). Another effect of E_{\max} is that the positive and negative peaks in ΔT_ε were shifted to higher temperatures.

Figure 3(c) and (d) show P_r and ΔT_{P_r} with E_{\max} ranging from 100 to 1,000 V/mm. The values of both P_r and ΔT_{P_r} increased with increasing E_{\max} ; the peak temperature of ΔT_{P_r} increased by about 1.5 K over this range of E_{\max} .

The $\Delta T_{\text{indirect}}$ value for each E_{\max} value is presented in Figure 4(a). As expected, increased E_{\max} resulted in increased $\Delta T_{\text{indirect}}$ and peak temperature. Figure 4(b) shows ΔT_{direct} , which well reproduces the intensities and peak temperature shifts of $\Delta T_{\text{indirect}}$. The relative contributions of ε and P_r depends on T and E_{\max} . Near T_m , the peak magnitude of the $\Delta T_{\text{indirect}}$ is governed by the peak magnitude of ΔT_{P_r} . This feature is unchanged even when the E_{\max} value changes. In contrast, the ΔT_ε contribution is important at $T > T_m$. Figure 4(c) shows the ratio of ΔT_ε to $\Delta T_{\text{indirect}}$ above T_m . Near T_m , the ratio is zero, indicating the dominance of ΔT_{P_r} in $\Delta T_{\text{indirect}}$. When T increases, the ratio increases and exceeds 0.5 because the greater E_{\max} decreases the ratio.

Summarizing, the overall ΔT was quantified by incorporating P_r and ε into the Maxwell relation. The overall ΔT near the T_m was governed by the contribution of P_r , while the contribution of ε was small. The contribution of ε steadily increased with temperature, and the ratio of ΔT_ε and overall ΔT

increased to about 0.5 above T_m . These behaviors indicate that to increase the magnitude of ΔT derived from the ECE, it is necessary to increase $\partial P_r/\partial T$ near T_m . To expand the ECE operating temperature range, it is necessary to adjust $\partial \varepsilon/\partial T$. To design ECE materials, their P_r and ε must be selected according to the required ECE characteristics. We expect that the results of this study will stimulate the search for ECE materials and thereby advance the development of micro-cooling devices.

Acknowledgement

The authors thank K. Uchida, T. Hirai, and M. Isomura for the equipment and technical support. This work was partially supported by Aid for Scientific Research (B) (24K01334, 24K01162), Aid for Scientific Research (S) (22H04965), and NIMS Joint Research Hub Program.

Figure caption

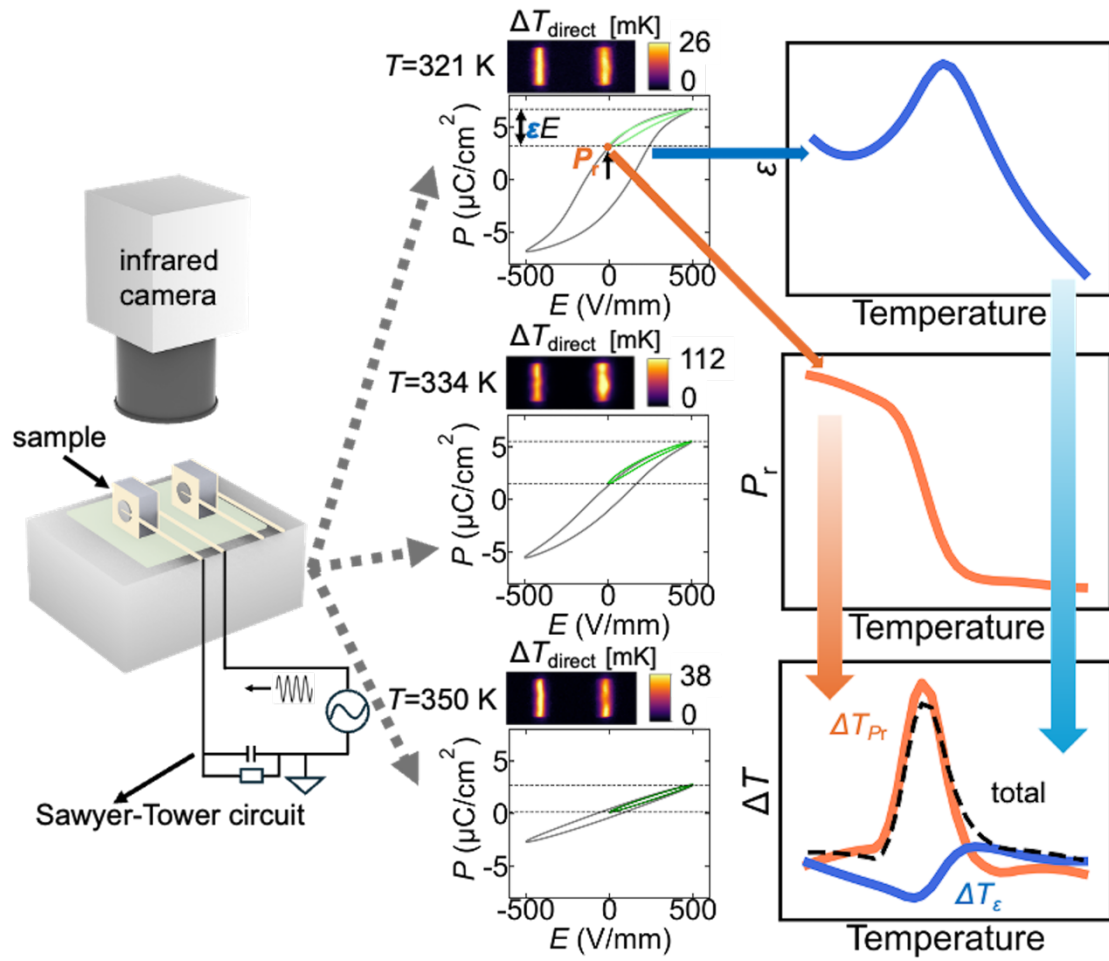


Figure 1. Experimental setup for LIT measurement and Sawyer Tower circuit. Thermal image, P - E hysteresis and indirect ΔT_{Pr} , ΔT_{direct} and overall ΔT with temperature were incorporated into the figure.

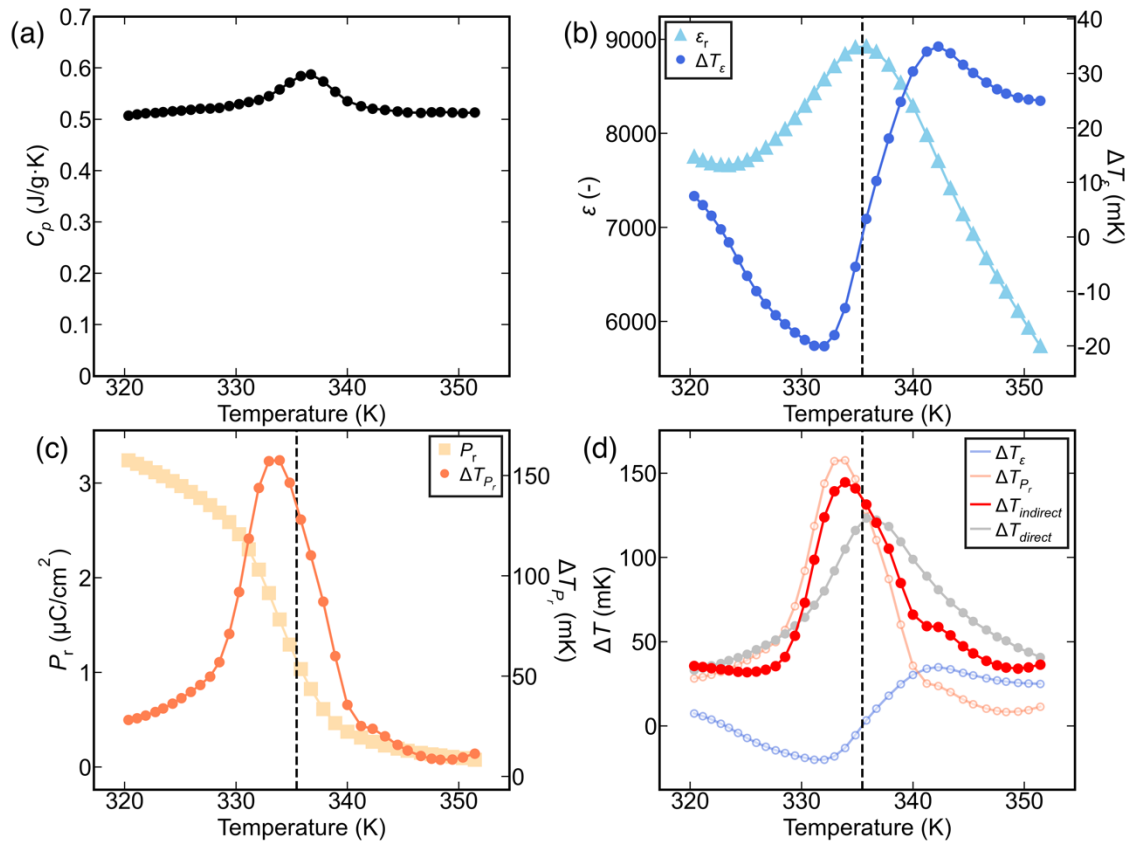


Figure 2. T -dependences of (a) ϵ and ΔT_ϵ , (b) P_r and ΔT_{P_r} at $E_{max}=500\text{V/mm}$ and (c) the comparison between $\Delta T_{indirect}$ ($\Delta T_\epsilon + \Delta T_{P_r}$) and the ΔT_{direct} measured by the LIT.

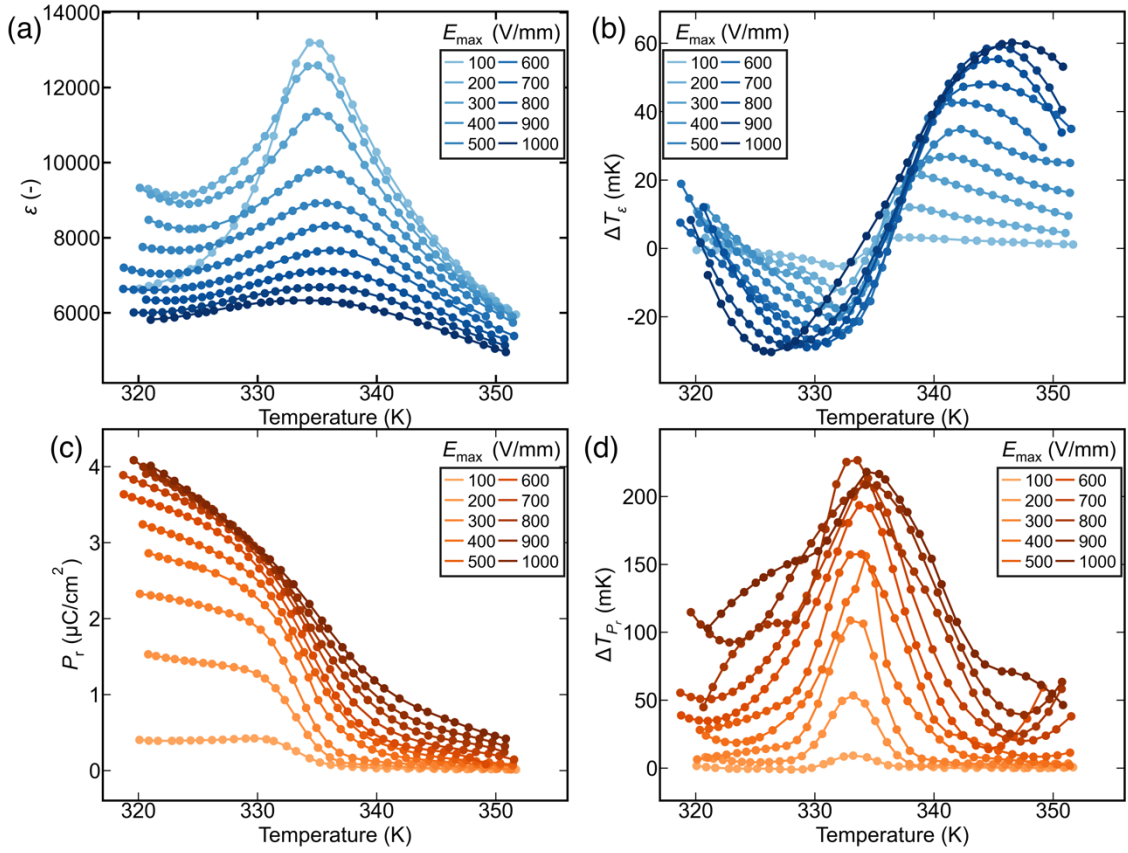


Figure 3. T -dependences of (a) ϵ , (b) ΔT_ϵ , (c) P_r and (d) ΔT_{P_r} at various E_{\max}

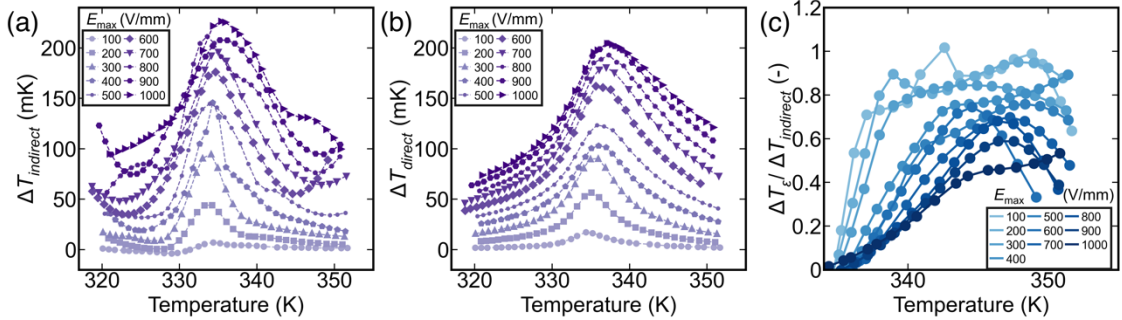


Figure 4. T -dependences of (a) the $\Delta T_{\text{indirect}}$, (b) the ΔT_{direct} at various E_{\max} and (c) the ΔT_ϵ contribution ratio to the total $\Delta T_{\text{indirect}}$ above the T_m .

AUTHOR DECLARATIONS

Conflict of Interest

The authors have no conflicts to disclose.

DATA AVAILABILITY

The data that support the findings of this study are available from the corresponding authors upon reasonable request.

References

- ¹E. Defay, R. Faye, G. Despesse, H. Strozyk, D. Sette, S. Crossley, X. Moya and N. D. Mathur, *Nat. Commun.* **9**, 1827 (2018).
- ²J. Li, A. Torelló, V. Kovacova, U. Prah, A. Aravindhnan, T. Granzow, T. Usui, S. Hirose and E. Defay, *Science* **382**, 801 (2023).
- ³B. Neese, B. Chu, S. G. Lu, Y. Wang, E. Furman, and Q. M. Zhang, *Science* **321**, 821 (2008).
- ⁴J. F. Scott, *Annu. Rev. Mater. Res.* **41**, 229 (2011).
- ⁵M. Valant, *Prog. Mater. Sci.* **57**, 980 (2012).
- ⁶S. G. Lu, B. Rozic, Q. M. Zhang, Z. Kutnjak and R. Pirc, *Appl. Phys. A* **107**, 559 (2012).
- ⁷B. Peng, H. Fan and Q. Zhang, *Adv. Funct. Mater.* **23**, 2987 (2013).
- ⁸X. Moya, S. Kar-Narayan and N. D. Mathur, *Nat. Mater.* **13**, 439 (2014).
- ⁹Y. Zhao, X. Hao and Q. Zhang, *J. Mater. Chem. C* **3**, 1694 (2015).
- ¹⁰A. S. Mischenko, Q. Zhang, J. F. Scott, R. W. Whatmore, and N. D. Mathur, *Science* **311**, 1270 (2006).
- ¹¹Y. S. Ju, *J. Electron. Packag.* **132**, 041004 (2010).
- ¹²R. Ma, Z. Zhang, K. Tong, D. Huber, R. Kornbluh, Y. S. Ju and Q. Pei, *Science* **357**, 1130 (2017).
- ¹³J. Shi, D. Han, Z. Li, L. Yang, S. G. Lu, Z. Zhong, J. Chen, Q. M. Zhang and X. Qian, *Joule* **3**, 1200 (2019).
- ¹⁴X. Moya, E. Stern-Taulats, S. Crossley, D. González-Alonso, S. Kar-Narayan, A. Planes, L. Mánosa, and N. D. Mathur, *Adv. Mater.* **25**, 1360 (2013).
- ¹⁵T. Yamada, S. Matsuo, T. Kamo, H. Funakubo, M. Yoshino, and T. Nagasaki, *Jpn. J. Appl. Phys.* **56**, 10PF15 (2017).
- ¹⁶J. Li, A. Torelló, Y. Nouchokgwe, T. Granzow, V. Kovacova, S. Hirose and E. Defay, *J. Phys. Energy* **5**, 024017 (2023).
- ¹⁷X. Chen, S. Li, X. Jian, Y. Hambal, S. G. Lu, V. V. Shvartsman, D. C. Lupascu and Q. M. Zhang, *Appl. Phys. Lett.* **118**, 122904 (2021).
- ¹⁸F. L. Goupil, A. Berenov, A. K. Axelsson, M. Valant and N. M. Alford, *J. Appl. Phys.* **111**, 124109 (2012).

- ¹⁹E. Birks, M. Dunce, J. Peräntie, J. Hagberg and A. Sternberg, *J. Appl. Phys.* **121**, 224102 (2017).
- ²⁰S. Zhang, J. Deliyore-Ramírez, S. Deng, B. Nair, D. Pesquera, Q. Jing, M. E. Vickers, S. Crossley, M. Ghidini, G. G. Guzmán-Verri, X. Moya and N. D. Mathur, *Nat. Mater.* **23**, 639 (2024).
- ²¹Y. Hirayama, R. Iguchi, X.-F. Miao, K. Hono, and K. Uchida, *Appl. Phys. Lett.* **111**, 163901 (2017).
- ²²R. Modak, R. Iguchi, H. Sepehri-Amin, A. Miura, and K. Uchida, *AIP Adv.* **10**, 065005 (2020).
- ²³R. Iguchi, D. Fukuda, J. Kano, T. Teranishi, and K. Uchida, *Appl. Phys. Lett.* **122**, 082903 (2023).
- ²⁴S. Matsuo, T. Yamada, T. Kamo, H. Funakubo, M. Yoshino and T. Nagasaki, *J. Ceram. Soc. Japan* **125**, 441 (2017).
- ²⁵M. Krupska-Klimczak, K. Ziewiec and I. Jankowska-Sumara, *Materials* **17**, 3329 (2024).
- ²⁶T. Yoshimura and N. Fujimura, *Jpn. J. Appl. Phys.* **42**, 6011 (2003).
- ²⁷R. Chukka, S. Vandrangi, S. Shannigrahi and L. Chen, *EPL* **103**, 47011 (2013).
- ²⁸S. Crossley, R. W. Whatmore, N. D. Mathur and X. Moya, *APL Mater.* **9**, 010701 (2021).
- ²⁹T. Teranishi, T. Sogabe, H. Hayashi, A. Kishimoto, and K. Fujimori, *Jpn. J. Appl. Phys.* **52**, 09KF06 (2013).
- ³⁰R. Pirc and R. Blinc, *Phys. Rev. B* **70**, 134107 (2004).
- ³¹D. A. Hall, M. M. Ben-Omran, and P. J. Stevenson, *J. Phys.: Condens. Matter* **10**, 461 (1998).
- ³²T. Teranishi, R. Ozaki, S. Kondo, and A. Kishimoto, *Jpn. J. Appl. Phys.* **62**, SM1015 (2023).
- ³³D. M. Marincel, H. Zhang, S. Jesse, A. Belianinov, M. B. Okatan, S. V. Kalinin, W. M. Rainforth, I. M. Reaney, C. A. Randall and S. Trolier-McKinstry, *J. Am. Ceram. Soc.* **98**, 1848 (2015).
- ³⁴R. Inoue, S. Ishikawa, R. Imura, Y. Kitanaka, T. Oguchi, Y. Noguchi and M. Miyayama, *Sci. Rep.* **5**, 14741 (2015).